This article was downloaded by:
On: *25 January 2011*
Access details: *Access Details: Free Access*
Publisher *Taylor & Francis*
Informa Ltd Registered in England and Wales Registered Number: 1072954 Registered office: Mortimer House, 37-41 Mortimer Street, London W1T 3JH, UK

Liquid Crystals
Publication details, including instructions for authors and subscription information:
http://www.informaworld.com/smpp/title~content=t713926090

Adaptive solution of a one-dimensional order reconstruction problem in Q-tensor theory of liquid crystals

Alison Ramage[a]; Christopher J. P. Newton[b]
[a] Department of Mathematics, University of Strathclyde, Glasgow G1 1XH, Scotland [b] Hewlett-Packard Labs, Bristol BS34 8QZ, England

To cite this Article Ramage, Alison and Newton, Christopher J. P.(2007) 'Adaptive solution of a one-dimensional order reconstruction problem in Q-tensor theory of liquid crystals', Liquid Crystals, 34: 4, 479 — 487
To link to this Article: DOI: 10.1080/02678290701267571
URL: http://dx.doi.org/10.1080/02678290701267571

PLEASE SCROLL DOWN FOR ARTICLE

Full terms and conditions of use: http://www.informaworld.com/terms-and-conditions-of-access.pdf

This article may be used for research, teaching and private study purposes. Any substantial or systematic reproduction, re-distribution, re-selling, loan or sub-licensing, systematic supply or distribution in any form to anyone is expressly forbidden.

The publisher does not give any warranty express or implied or make any representation that the contents will be complete or accurate or up to date. The accuracy of any instructions, formulae and drug doses should be independently verified with primary sources. The publisher shall not be liable for any loss, actions, claims, proceedings, demand or costs or damages whatsoever or howsoever caused arising directly or indirectly in connection with or arising out of the use of this material.

Liquid Crystals, Vol. 34, No. 4, April 2007, 479–487

Taylor & Francis
Taylor & Francis Group

Adaptive solution of a one-dimensional order reconstruction problem in Q-tensor theory of liquid crystals

ALISON RAMAGE*† and CHRISTOPHER J. P. NEWTON‡

†Department of Mathematics, University of Strathclyde, Glasgow G1 1XH, Scotland
‡Hewlett-Packard Labs, Filton Road, Stoke Gifford, Bristol BS34 8QZ, England

(*Received 7 September 2006; in final form 14 December 2006; accepted 14 December 2006*)

In this paper we illustrate the suitability of an adaptive moving mesh method for modelling a one-dimensional liquid crystal cell using **Q**-tensor theory. Specifically, we consider a time-dependent problem in a Pi-cell geometry which admits two topologically different equilibrium states and model the order reconstruction which occurs on the application of an electric field. An adaptive finite element grid is used where the grid points are moved according to equidistribution of a monitor function based on a specific property of the **Q**-tensor. We show that such moving meshes provide the same level of accuracy as uniform grids but using far fewer points, and that inaccurate results can be obtained if uniform grids are not sufficiently refined.

Downloaded At: 15:44 25 January 2011

1. Introduction

External influences such as bounding surfaces or an applied electric field can induce changes in director orientation in a liquid crystal cell. Changes in the scalar order parameters are less usual in classical liquid crystal cells, but in regions where distortion of the director occurs over small length scales (10–100 nm), the molecular order may be significantly altered. The consequential effect on the optical and, in particular, switching properties of the liquid crystal system is of key importance, and has become increasingly so in recent years with the development of the zenithal bistable nematic (ZBN) [1, 2] and Pi-cell [3]. It is therefore crucial that the behaviour and nature of these defects can be accurately represented by any numerical model.

The nematic liquid crystal phase can be modelled mathematically by the director, a unit vector **n** in the direction of the local preferred alignment, and a measure of how ordered the molecules are in this direction, the scalar order parameter S [4]. Although this uniaxial description is sufficient for the majority of situations, the most general configuration of molecules in a nematic material is a biaxial state. To describe this state, it is necessary to specify two directors (**n** and **m**) and two scalar order parameters (S_1 and S_2). A static theory of nematic liquid crystals which allows for changes in the scalar order parameters (but does not include fluid flow) was developed from the theory of Landau by de Gennes [5]. In this case, minimization of the total free energy of a liquid crystal sample leads to a set of five coupled differential equations for the five degrees of freedom of the order parameter tensor **Q**, which is the symmetric traceless second rank tensor defined by

$$\mathbf{Q} = S_1(\mathbf{n}\otimes\mathbf{n}) + S_2(\mathbf{m}\otimes\mathbf{m}) - \frac{1}{3}(S_1+S_2)\mathbf{I} \qquad (1)$$

where $\boldsymbol{I}$ is the identity matrix [5]. A detailed description of this model can be found in [6]. More recently, extensions of this theory have been proposed by Beris and Edwards [7], Olmsted and Goldbart [8] and Sonnet *et al*. [9].

One advantage of a **Q**-tensor (as opposed to a director-based) description is that topological defects do not appear as mathematical singularities. This means that relatively unsophisticated numerical methods can often be used to model certain simple configurations, particularly in the context of identifying static equilibrium states. A number of authors have previously presented numerical studies in this vein, using finite difference discretizations on uniform grids to calculate steady state solutions. For example Schopohl and Sluckin investigated the core structure of half-integer wedge disclinations in a two-dimensional region [10]; the conversion of a reverse tilt wall to a pair of disclination lines was modelled by Lee *et al.* [11], and Sonnet *et al.* [12] proposed a method using a finite difference discretization with a one-step

*Corresponding author. Email: A.Ramage@strath.ac.uk

Liquid Crystals
ISSN 0267-8292 print/ISSN 1366-5855 online © 2007 Taylor & Francis
http://www.tandf.co.uk/journals
DOI: 10.1080/02678290701267571

SOR-Newton method which performed well in both two and three dimensions. In terms of other discretizations, finite element analysis of the Landau–de Gennes minimization problem was presented by Davis and Gartland [13]. Gartland *et al.* have computed elastic forces on nematic point defects using nonuniform grids of triangular elements [14]. A scheme based on the adaptive finite element mesh refinement work of Oden *et al.* [15] was used by Fukada and coworkers for modelling static defect structure for certain axisymmetric geometries in two and three dimensions [16, 17]. The static configuration of defects in a two-dimensional representation of a ZBN device has recently been investigated numerically by Mottram and Newton [6], again using spatially-adaptive finite elements.

In addition to the defect core structure, the dynamics of defect movement is also a crucial issue for liquid crystal cells. Numerical simulations of such effects are much less common in the current research literature. Barberi *et al.* [18] recently used a one-dimensional numerical model to investigate the dynamics of the biaxial switching of a nematic cell subjected to a strong electric field. The thesis of Svensek [19] studies the dynamics of the order parameter coupled to hydrodynamics in two dimensions, but using director theory rather than the **Q**-tensor approach proposed here. Both of these works use standard finite difference discretizations on uniform grids. However, the presence in the physical problem of characteristic lengths with large scale differences (the size of the defect is very small compared with that of the cell) suggests that more sophisticated numerical modelling techniques could be used here to great effect.

One obvious approach is to use an adaptive grid technique, ensuring that there is no waste of computational effort in areas where there is no need for a fine grid. Adaptive grid methods have been successfully used to solve partial differential equations (PDEs) in many branches of computational mathematics such as computational fluid dynamics, mathematical biology, semiconductor modelling and aerospace engineering (see, for example, [20–25]). In this paper we present an introductory study of the use of adaptive grid methods for solving PDE problems in **Q**-tensor theory of liquid crystals. Specifically, we consider the time-dependent order reconstruction problem studied in [18] which requires the solution of six coupled PDEs. We illustrate the feasibility of using a moving mesh adaptive grid technique and show that it has advantages in terms of accuracy and efficiency over using a uniform grid with the same number of points.

2. Basic Q-tensor theory

A full account of the director-based mathematical theory of liquid crystals can be found in [26]. An expression for the free energy density of the form

$$\mathcal{F} = \int_V F(\theta, \phi, \nabla\theta, \nabla\phi)\mathrm{d}V + \int_S F(\theta, \phi)\mathrm{d}S$$

can be derived, where V is the volume and S is the surface of the liquid crystal region. The problem of finding the minimum energy can then be tackled using a calculus of variations approach. This theory assumes that the liquid crystal is uniaxial and that the order is constant throughout. In cases where order variations are important (for example, in the ZBN display where defects stabilize one of the states) the order can be explicitly included by introducing the scalar order parameter, S, or implicitly by using the tensor order parameter, **Q**, as defined in [1]. Using the **Q**-tensor removes the assumption that the material is uniaxial and it is this more general approach that we use here.

In general, **Q** can be represented by a symmetric traceless matrix as

$$\mathbf{Q} = \begin{bmatrix} q_1 & q_2 & q_3 \\ q_2 & q_4 & q_5 \\ q_3 & q_5 & -q_1 - q_4 \end{bmatrix} \tag{2}$$

involving the 5 quantities q_i, $i=1, \ldots, 5$. If it is assumed that distortions of **Q** are small, the resulting $\mathcal{F}$ can be taken to depend only on **Q** and its first derivatives, that is,

$$\mathcal{F} = \int_V F_{\mathrm{bulk}}(q_i, \nabla q_i)\mathrm{d}v + \int_S F_{\mathrm{surface}}(q_i)\mathrm{d}s.$$

Full details of this process can be found in, for example, [6]. If fixed boundary conditions are applied (strong anchoring), the surface energy term can be ignored in the minimization. Taking the elastic energy up to second order in the gradient of **Q**, the bulk energy can be written as $\mathcal{F}_{\mathrm{bulk}} = F_{\mathrm{thermotropic}} + F_{\mathrm{elastic}} \equiv F_{\mathrm{t}} + F_{\mathrm{e}}$, with

$$\begin{aligned} F_{\mathrm{t}} &= \frac{1}{2}A(T - T^*)\mathrm{tr}\,\mathbf{Q}^2 - \frac{\sqrt{6}}{3}B\,\mathrm{tr}\,\mathbf{Q}^3 + \frac{1}{4}C\left(\mathrm{tr}\,\mathbf{Q}^2\right)^2 \\ F_{\mathrm{e}} &= \frac{1}{2}L_1(\mathrm{div}\,\mathbf{Q})^2 + \frac{1}{2}L_2|\nabla \times \mathbf{Q}|^2 \end{aligned} \tag{3}$$

where A, B, C, L_1 and L_2 are positive constants, T represents temperature and T^* is the pseudocritical temperature at which the isotropic phase becomes unstable (see [27]). Estimates for these material parameters can be obtained from the literature.

For computational purposes, it is useful to nondimensionalize the equations (3) with respect to the

Downloaded At: 15:44 25 January 2011

Downloaded At: 15:44 25 January 2011

nematic coherence length $\zeta = \left[9CL_2/\left(2B^2\right)\right]^{\frac{1}{2}}$. The values for material constants used throughout this paper (taken from [18]) are: $L_1 = 9.7 \times 10^{-12}$ N, $L_2 = 2.4 \times 10^{-12}$ N, $A = 0.13 \times 10^6$ J K^{-5} m^{-3}, $B = 1.6 \times 10^6$ J K^{-5} m^{-3}, $C = 3.9 \times 10^6$ J K^{-5} m^{-3}; giving $\zeta = 4.06 \times 10^{-9}$. Using a value of T–$T^* = -0.38$°C results in the scaled parameters (which we will denote with $_s$) $L_{1s} = 4.0417$, $A_s = -0.33682$, $B_s = 10.969$ and $C_s = 26.736$.

3. Adaptive grid methods

It is well known in the numerical analysis community that adaptive or moving mesh methods are capable of resolving solutions with sharp transitions such as boundary layers to acceptable degrees of accuracy without using an excessive number of grid points. The two main strategies in common use are local mesh refinement (known as h or p refinement), where extra nodes are added on a local basis in regions of high error, and mesh movement (r refinement), where existing grid points are moved to regions of high errors while maintaining the same grid connectivity. In this paper, we consider the latter approach. For these methods, the adaptive grid is generally constructed as the image under a suitably defined mapping of a fixed mesh over an auxiliary domain. The advantages include relatively simple implementation, comparatively easy extension of existing software for fixed mesh methods, and minimal numerical diffusion and dispersion (that is, the shape and speed of time-dependent features of the solution are accurately reproduced).

As stated above, r refinement adaptive methods use non-uniform grids which, as time evolves, concentrate grid points in spatial regions of high activity and follow the features of the computed solution. One common theme of many such adaptive methods is the idea of *equidistribution*, introduced by de Boor [28] for solving boundary value problems for ODEs. The idea is to select grid points in order to limit some measure of the solution error (defined using a *monitor function*) by distributing it equally across each subinterval. Many different ways of generating adaptive methods based on equidistribution principles have been developed, via both discrete moving mesh equations (which are systems of ODEs) and continuous moving mesh equations (so-called moving mesh PDEs, or MMPDEs). Here we illustrate the ideas involved for a simple PDE in one dimension.

Suppose we are solving on a physical domain $\Omega_p \equiv [0, 1]$ for an unknown function $u(z, t)$. To generate a grid, we look for a mapping from computational space $\Omega_c \times (0, T]$ say (where Ω_c is usually taken to be the same as Ω_p) to physical space $\Omega_p \times (0, T]$ such that, in the transformed variables, the variation of the selected monitor function is reduced. For example, if z and ξ denote the physical and computational coordinates, respectively, a one-to-one coordinate transformation between the domains is denoted by

$$z = z(\xi, t), \qquad \xi \in \Omega_c = (0, 1), \qquad t \in (0, T]$$
$$z(0) = 0, \qquad z(1) = 1.$$

We impose a uniform mesh on the computational domain, given by

$$\xi_i = \frac{i}{N}, \qquad i = 0, 1, \ldots, N$$

where N is a positive integer, and denote the corresponding mesh in Ω_p by

$$0 = z_0(t) < z_1(t) < \ldots < z_{N-1}(t) < z_N(t) = 1.$$

For a chosen monitor function $M(u(z, t))$, the one-dimensional *equidistribution principle* (EP) can be expressed as

$$\int_0^{z(\xi, t)} M(u(s, t))\mathrm{d}s = \xi \int_0^1 M(u(s, t))\mathrm{d}s. \tag{4}$$

This EP can be expressed equivalently in discrete form as

$$\int_{z_i(t)}^{z_{i+1}(t)} M(u(s, t))\mathrm{d}s = \int_{z_{i-1}(t)}^{z_i(t)} M(u(s, t))\mathrm{d}s, \quad i = 1, \ldots, N-1$$

or

$$\int_{z_{i-1}(t)}^{z_i(t)} M(u(s, t))\mathrm{d}s = \frac{1}{N}\int_0^1 M(u(s, t))\mathrm{d}s, \quad i = 1, \ldots, N. \tag{5}$$

We also note in passing that differentiating (4) once with respect to ξ gives a differential form of the EP,

$$M(z(\xi, t))\frac{\partial}{\partial \xi} z(\xi, t) = \int_0^1 M(u(s, t))\mathrm{d}s$$

which can be regarded as an MMPDE.

One major issue associated with the generation of adaptive grids based on an equidistribution principle is the choice of a suitable monitor function. This is particularly true for complicated PDEs and in higher dimensions. For the one-dimensional (1D) problems considered here, we restrict our attention to one of the standard methods and choose M to be a measure of the arc-length of a specified quantity, here the solution $u(z)$. That is, we take

$$M(u(z, t)) = \left[\mu + \left(\frac{\partial u}{\partial z}(z, t)\right)^2\right]^{\frac{1}{2}} \tag{6}$$

where μ is a user-prescribed scaling parameter.

Examples of the use of other monitor functions for 1D problems can be found in [29–31].

The overall adaptive solution process has two key components, namely, the generation of a grid and the solution of the physical differential equation(s) on that grid. For a general multi-dimensional time-dependent problem, this can be considered as an iterative process with two main steps: (1) a mesh is generated using equidistribution (based on the numerical solution at the current time step); (2) the physical PDEs are solved on the new mesh to produce the solution at the new time level.

At time $t=0$, the grid points are uniformly distributed. In this paper, step 1 is implemented using the method presented by Sanz-Serna and Christie [32], which is equivalent to equidistributing the arc-length monitor function given by equation (6) over the interval [0, 1]. Step 2, and the advancement of the solution in time, is carried out using the COMSOL Multiphysics finite element package [33]. Specifically, at each time step the physical PDEs are solved using finite element approximation with quadratic elements. The solution u is then updated in time via one step of the COMSOL time-dependent solver, femtime.

4. A one-dimensional model problem

In this section we summarize the results in [34] where a simple uniaxial 1D model problem is used to assess the accuracy and efficiency of an adaptive grid technique. The problem involves a sample with homogeneous uniaxial alignment in the one-dimensional domain $\Omega_s \equiv z \in [0,\ d_s]$, where the domain has been scaled in accordance with the non-dimensionalization adopted in § 2; that is, the true length of the physical domain is d μm microns where $d=d_s\zeta$. For uniaxial problems with the z-axis in the direction of $\mathbf{n}$, (1) becomes

$$\mathbf{Q}=\sqrt{\frac{3}{2}}S\begin{bmatrix}-\frac{1}{3} & 0 & 0\\ 0 & -\frac{1}{3} & 0\\ 0 & 0 & \frac{2}{3}\end{bmatrix}$$

so that $\mathbf{Q}$ depends only on the scalar order parameter S, with $\mathrm{tr}\,(\mathbf{Q}^2)=S^2$. As a result, the free energy density can be minimized by solving a single Euler–Lagrange equation for S, subject to suitable boundary conditions. Furthermore, the expressions for the energies in equation (3) simplify to

$$F_t=\frac{1}{2}A_sS^2-\frac{1}{3}B_sS^3+\frac{1}{4}C_sS^4,\qquad F_e=\left(\frac{2L_{1s}+1}{6}\right)\left(\frac{\partial S}{\partial z}\right)^2 \quad (7)$$

so the governing differential equation for S is therefore the Euler–Lagrange equation

$$S''=\alpha S-\beta S^2+\gamma S^3,\quad \alpha=\frac{3A_s}{2L_{1s}+1},\quad \beta=\frac{3B_s}{2L_{1s}+1},\quad \gamma=\frac{3C_s}{2L_{1s}+1}. \quad (8)$$

This is solved subject to the boundary conditions $S=0$ at $z=0$ and $S=S_{eq}$ at $z=d_s$. The equilibrium nematic scalar order parameter S_{eq} (which minimizes (7)) given by $S_{eq}=\left[B_s+\sqrt{B_s^2-4A_sC_s}\,\right]/2C_s$. Approximations to the exact solutions of equation (8) (calculated using numerical integration) for regions of length $d=0.1$, 1, 10 μm are plotted in figure 1 (for clarity, these plots show $z \in [0,\ d/2]$ only). In each case, the solution features a boundary layer of width approximately 25 nm, which occupies a smaller proportion of the total cell length as d increases.

To resolve these layers accurately on a finite element (or finite difference) grid, a high concentration of grid points is required in the boundary layer. With a uniform grid, this means that the grid must be highly refined throughout the domain, thus wasting much

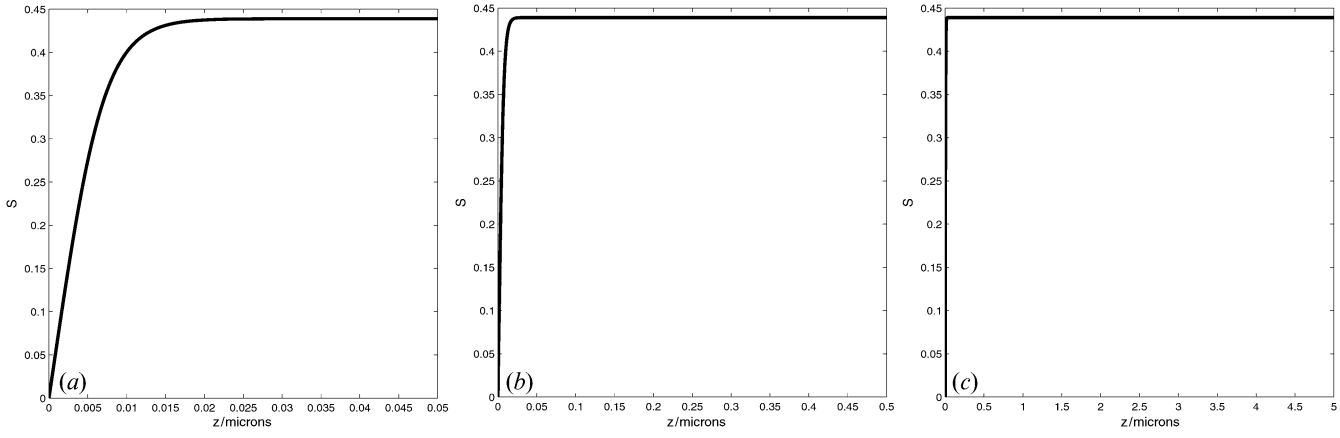

Figure 1. Plot of order parameter S for domains of varying length. For clarity, the right-hand half of each domain has been omitted: (*a*) $d=0.1$ μm, (*b*) $d=1$ μm, (*c*) $d=10$ μm.

Downloaded At: 15:44 25 January 2011

computational effort. Here we seek a suitable adaptive grid by equidistributing the solution arc-length in order to move grid points into the boundary layer. Specifically, we use the adaptive algorithm described above with monitor function

$$M(S(z,t)) = \left[1 + \left(\frac{\mathrm{d}S}{\mathrm{d}z}(z,t)\right)^2\right]^{\frac{1}{2}}.$$

As this is a stationary problem, we introduce a 'false' timescale and apply the iteration until the grid points are no longer moving with time; that is, until the grid has reached a steady state distribution. The resulting mesh trajectories (plotted against time) with $N=64$ and $d=1\,\mu$m are shown in figure 2 (*a*). Figure 2 (*b*) shows a magnification of the trajectories over the first ten time steps (the time step size is $\delta t = 1e{-}6$). It can be seen that the node points move very quickly in response to the presence of the boundary layer.

By considering the error incurred when the exact solution to a closely related problem is approximated by its linear interpolant, it can also be shown that we expect the adaptive grid obtained to exhibit the same rate of uniform convergence as a uniform grid with the same number of points [34]. In addition, the errors incurred with uniform and adaptive grids for the model problem above can be quantified by comparing computed solutions with a numerical solution calculated using a very fine uniform grid and using linear interpolation to obtain the values of this fine grid solution at the current grid points. The results in [34] show that where it can be accurately measured, the error with the adaptive grid is smaller than the error with a uniform grid with the same number of points. That is, a smaller number of points are required to achieve a fixed order of accuracy with an adaptive grid rather than a uniform one. Furthermore, a comparison of CPU times shows that the cost of calculating the adaptive grid is not prohibitive and the relative efficiency of the adaptive method improves as higher accuracy (smaller tolerance) is required.

5. An order reconstruction example

In this section we consider a more realistic 1D example, namely the order reconstruction problem studied by Barberi *et al.* [18]. The geometry is that of the Pi-cell [35] and the liquid crystal parameters used are taken from [18], as described in § 2. At both boundaries, the cell surface is treated so as to induce alignments uniformly tilted by a specified *tilt angle*, θ_t, but oppositely directed. This set-up admits two topologically different equilibrium states: in one, there is a mostly horizontal alignment of the director with a slight splay; in the other, there is a mostly vertical alignment with a bend of almost π radians. Depending on the tilt angle and ratio of the elastic moduli, either of these states might have a lower elastic energy, but the energy barrier between

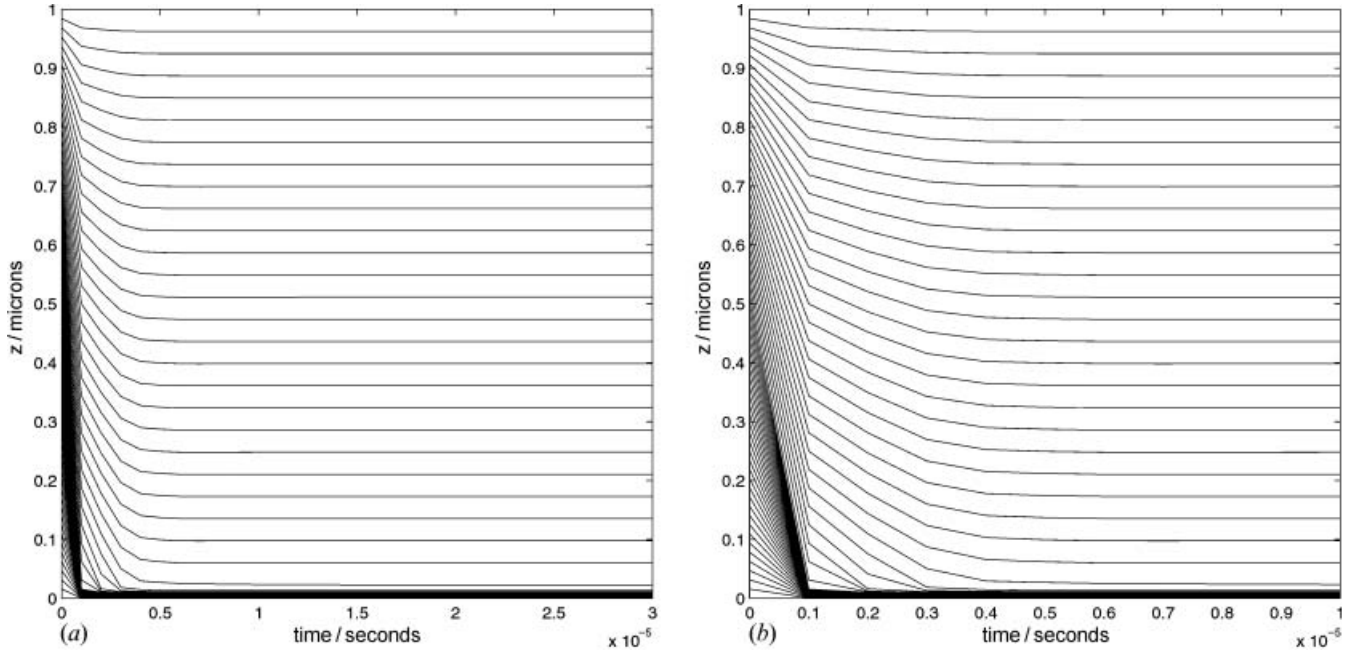

Figure 2. Mesh trajectories for $N=64$ and $d=1\,\mu$m. The plots shows the paths followed by each node as time evolves. (*a*) Node trajectories against time. (*b*) Magnification for first 10 time steps.

Downloaded At: 15:44 25 January 2011

them is always large enough to prevent a spontaneous transition. Here, an electric field is applied and the order reconstruction (which, from symmetry considerations, will take place in the centre of the cell) is modelled.

As this is not a purely uniaxial problem, we must consider the full **Q**-tensor (2). The resulting Euler–Lagrange equations are five coupled PDEs, corresponding to q_i, $i=1, \ldots, 5$. These must be solved in conjunction with an additional PDE for the electric potential U. These equations are cumbersome and will not be reproduced here: details can be found in [6, 18]. To monitor the order reconstruction, we use the invariant measure of biaxiality given in [18], that is,

$$b=\left[1-\frac{6\,\mathrm{tr}(Q^3)^2}{\mathrm{tr}(Q^2)^3}\right]^{\frac{1}{2}}. \tag{9}$$

The initial configuration has a tilt angle which varies linearly with z between θ_t and $-\theta_t$. A pulse of voltage V is applied at time $t=2\times10^{-3}$ s for a duration of 0.25 μs and the time step size is $\delta t=1\times10^{-7}$ s. When V is less than a critical value, the biaxiality in the centre increases, but when the field is switched off, the cell slowly relaxes back into its original state. However, when the applied voltage is high enough, the orientation in the centre becomes purely biaxial ($b=1$) and the transition to the mostly vertical state takes place.

In this case, the physical problem is modelled by six coupled PDEs so, unlike for the model problem in § 4, there is no simple solution on which to base an equidistribution principle. Here we replace $u(z, t)$ in equation (6) by $\mathcal{T}(z, t)=\mathrm{tr}(\mathbf{Q})^2$, that is, we use the monitor function

$$M(\mathcal{T}(z, t))=\left[1+\left(\frac{\mathrm{d}\mathcal{T}}{\mathrm{d}z}(z, t)\right)^2\right]^{\frac{1}{2}}.$$

The quantity $\mathcal{T}(z, t)$ is an appropriate choice here as it is known to vary rapidly in the neighbourhood where order reconstruction will occur, that is, where high resolution of the numerical solution is required. The Euler–Lagrange equations are solved at each time step using COMSOL quadratic finite element approximation as before, and the adaptive method used is the full time-dependent algorithm described in § 3.

In these experiments, we aim to mimic the results presented in [18]. We therefore consider a tilt angle of 20° and a region of length $d=1$ μm. Plots of equation (9) for the two voltages, $V=11.3$ and 11.32 V, which are sub- and super-critical, respectively, are shown in figures 3 (*a*) and 3 (*b*). These are comparable to figures 6 and 7 in [18] (although we have used 256 grid points in space as opposed to the 1000 used there). The node trajectories for the adaptive grids are shown in figure 4, where only every second grid point has been included for clarity. In figures 4 (*a*) and 4 (*b*), the voltage $V=11.3$ V is low enough for the cell to relax back to its initial configuration after the electric field is switched off, which is reflected in the grid paths. The right-hand plot is a magnification of what happens to the adaptive grid as this occurs. Similarly, figures 4 (*c*) and 4 (*d*) are associated with a voltage of $V=11.32$ V, which triggers a biaxial transition. The right-hand plot is a magnification of what happens to the node points when this transition takes place; namely, they reform a uniform grid.

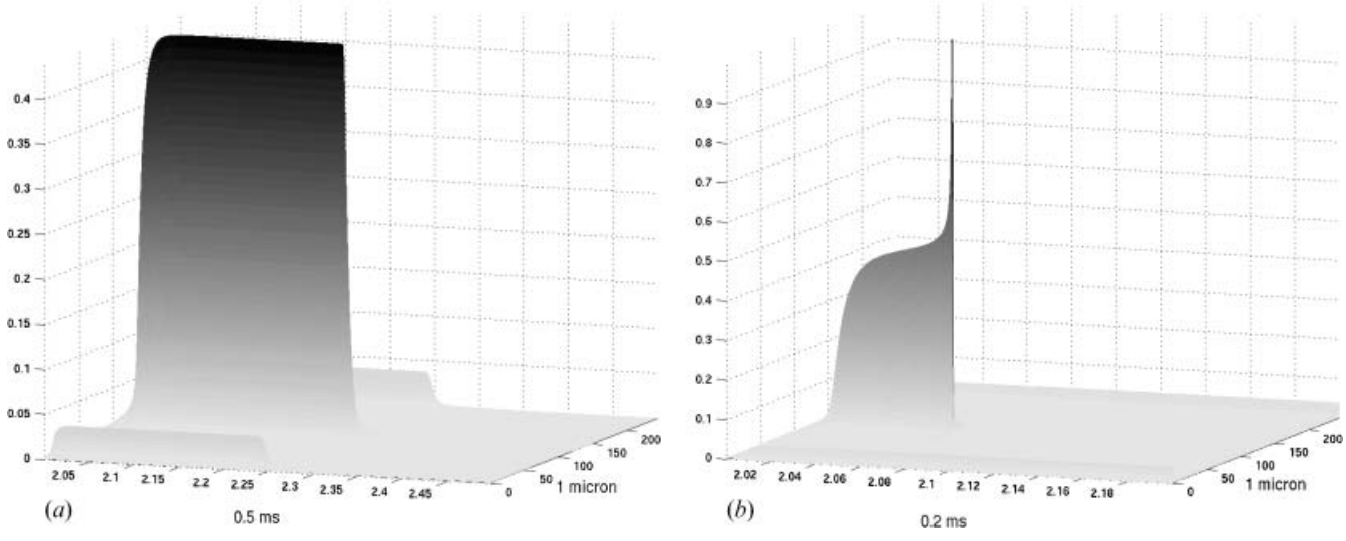

Figure 3. Plots of biaxiality at sub- and super-critical voltages: (*a*) $V=11.3$ V, (*b*) $V=11.32$ V.

Downloaded At: 15:44 25 January 2011

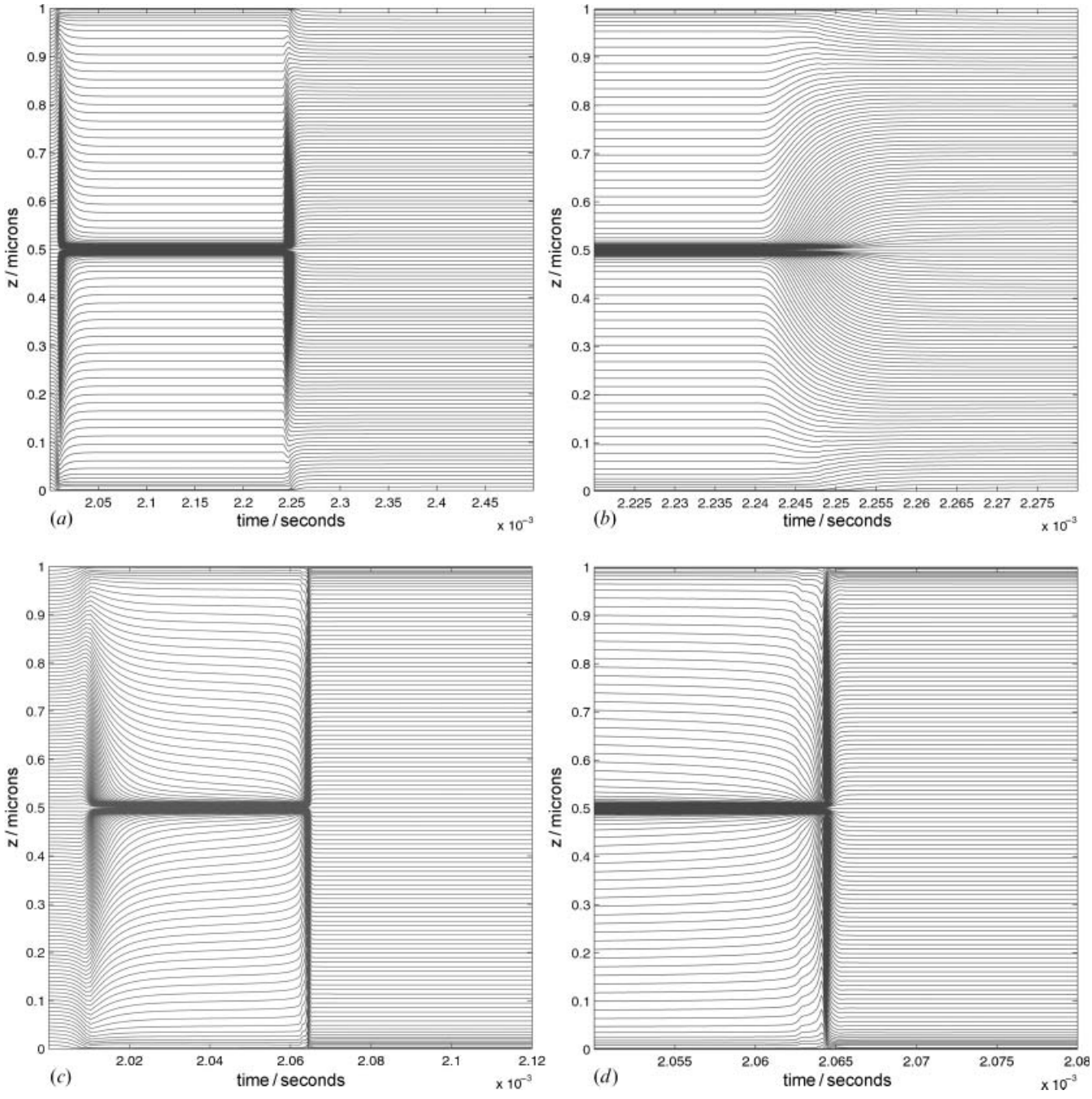

Figure 4. Adaptive grids trajectories for order reconstruction problem; each plot shows the paths followed by the nodes as time evolves. (*a*) Adaptive grid trajectories, $V=11.3$ V; (*b*) magnified grid trajectories as field is switched off, $V=11.3$ V; (*c*) adaptive grid trajectories, $V=11.32$ V; (*d*) magnified grid trajectories during biaxial transition, $V=11.32$ V.

When the applied voltage is high enough, the orientation in the centre becomes purely biaxial, so $b=1$ and transition to the vertical state takes place. At the cell centre, two eigenvalues of **Q** are exchanged. This exchange of eigenvalues is illustrated in figure 5 (cf. [[18], figure 8]). Figure 6 (*a*) shows a close-up of the structure in the centre of the cell, where the order reconstruction takes place on a timescale of a few μs. The biaxiality here actually has a volcano-like structure, with the base of the crater being a single point representing a planar uniaxial state with $b=0$ (this is where two eigenvalues of **Q** are equal and positive). The adaptive grid has clearly captured this feature accurately (cf. [[18], figure 9]). Figures 6 (*b*) and 6 (*c*) show

Downloaded At: 15:44 25 January 2011

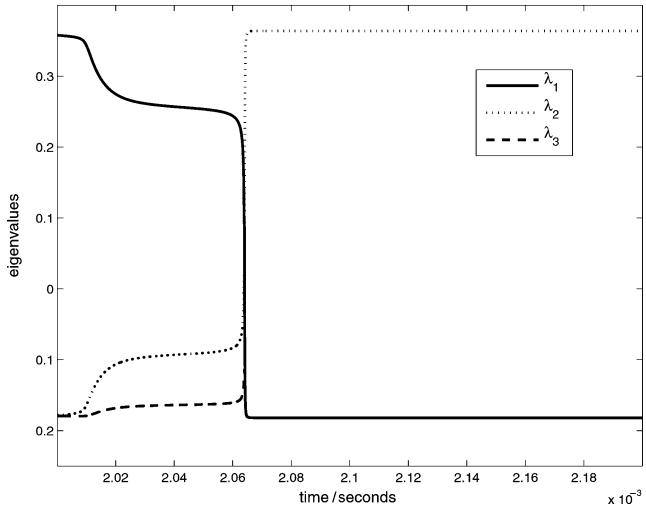

Figure 5. Eigenvalues of **Q** at the cell centre.

cross-sections of this structure at the cell centre when using a uniform grid and adaptive grid, respectively, both with $N=256$ points. The uniform grid has failed to capture the volcano's crater, but the adaptive grid represents the structure well, with b close to zero at the cell centre. In addition to this inaccuracy in the structure, the time at which switching occurs is also wrong when calculated using a uniform grid with 256 points. A full comparison of switching times is given in table 1. It can be seen that when the uniform grid is not fine enough, switching either does not occur at all or occurs at a later time. In contrast, the switching process is modelled correctly by a relatively coarse adaptive grid. In terms of the planar uniaxial point at the volcano's centre, a uniform grid with $N=1024$ gives a value of 3.28×10^{-1} while an adaptive grid with $N=128$ gives 2.37×10^{-1}. The latter is therefore giving a more

Table 1. Times at which switching occurs (in microseconds) when $V=11.32$ V.

N	Uniform	Adaptive
128	no switching occurs	2.064×10^{-3}
256	2.100×10^{-3}	2.064×10^{-3}
512	2.065×10^{-3}	2.064×10^{-3}
1024	2.064×10^{-3}	2.064×10^{-3}

accurate solution (measured in this sense) using 8 times fewer grid points.

As an indication of efficiency, we note that the overall time taken (in CPU seconds) for the full time-dependent calculation over time interval T was as follows: for $V=11.3$ V and $T=0.5\,\mu$s, the uniform grid of 1000 points took 1.5295×10^{4} s and the adaptive grid of 256 points took 9.8312×10^{3} s. For $V=11.32$ V and $T=0.2\,\mu$s, the uniform grid of 1000 points took 7.6918×10^{3} s and the adaptive grid of 256 points took 5.7618×10^{3} s. These figures indicate that the overhead from calculating the adaptive grid is not prohibitive and we still speed up the solution process by a significant amount.

6. Observations and conclusions

In this paper we have given an example of how adaptive grids can be used to solve one-dimensional problems in **Q**-tensor theory. The specific method used, i.e. that of equidistributing the arc-length of $\mathrm{tr}\,\mathbf{Q}^2$, proved to be very effective for a realistic order reconstruction problem involving the solution of six coupled PDEs. With an adaptive grid, we were able to reproduce the results of other authors [18] in a more efficient way using fewer computational resources. The moving meshes studied here provided the same level of accuracy

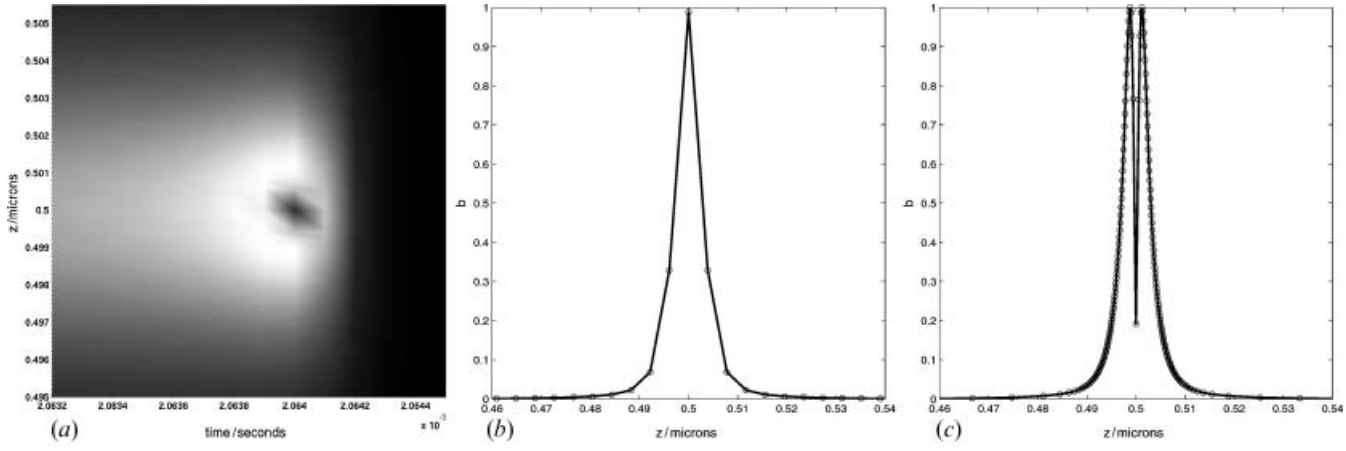

Figure 6. Detail of the biaxial transition at the cell centre measured using b in equation (9). (*a*) Contour plot of b at cell centre during transition; (*b*) uniform grid, $N=256$; (*c*) adaptive grid, $N=256$.

Downloaded At: 15:44 25 January 2011

as uniform grids, but using far fewer points, resulting in a computational saving. In addition, it was shown that using a uniform grid which is insufficiently fine led to incorrect modelling of the nature and timing of the switching process. We anticipate that these adaptive grid methods have the potential for similar gains in two- and three-dimensional problems.

Acknowledgement

This work was supported by EPSERC grant EP/C 53154 × /1.

References

[1] G. Bryan-Brown, C. Brown, J. Jones, E. Wood, I. Sage, P. Brett, J. Rudin. *SID Symp. Dig.*, **28**, 37 (1997).
[2] C.J. Newton, T. Spiller. In *SID Proceedings of IDRC97*, J. Morreale (Ed.), Santa Ana, CA, SID. p. 13 (1997).
[3] P. Bos, K. Beran. *Mol. Cryst. liq. Cryst.*, **113**, 329 (1984).
[4] E.G. Virga. *Variational Theories for Liquid Crystals*. Chapman and Hall, London (1994).
[5] P. de Gennes. An analogy between superconductors and smectics a *Solid State Commun.*, **10**, 753 (1972).
[6] N.J. Mottram, C.J. Newton. *Introduction to Q-tensor theory,* Tech. Rep. 10/04, University of Strathclyde (2004).
[7] A. Beris, B. Edwards. *Thermodynamics of Flowing Systems*. Oxford University Press, Oxford (1994).
[8] P. Olmsted, P. Goldbart. *Phys. Rev. A*, **46**, 4966 (1992).
[9] A.M. Sonnet, P.L. Maffettone, E.G. Virga. *J. non-Newtonian Fluid Mech.*, **119**, 51 (2004).
[10] N. Schopohl, T.J. Sluckin. *J. Phys. Fr.*, **49**, 1097 (1988).
[11] G.-D. Lee, J. Anderson, P. Bos. *Appl. Phys. Lett.*, **81**, 3951 (2002).
[12] A.M. Sonnet, A. Kilian, S. Hess. *Phys. Rev. E*, **52**, 718 (1995).
[13] T.A. Davis, E.C. Gartland. *SIAM J. Numer. Anal.*, **35**, 336 (1998).
[14] E.C. Gartland, A.M. Sonnet, E.G. Virga. *Continuum Mech. Thermodyn.*, **14**, 307 (2002).
[15] J. Oden, T. Strouboulis, P. Devloo. *Comput. Method Appl. M.*, **59**, 327 (1986).
[16] J. Fukuda, H. Yokoyama. *Eur. Phys. J. E*, **4**, 389 (2001).
[17] J. Fukuda, M. Yoneya, H. Yokoyama. *Phys. Rev. E*, **65**, art. no. 327 041709 (2002).
[18] R. Barberi, F. Ciuchi, G. Durand, M. Iovane, D. Sikharulidze, A.M. Sonnet, E.G. Virga. *Eur. Phys. J. E*, **13**, 61 (2004).
[19] D. Svensek. PhD thesis, University of Ljubljana, Slovenia (2001).
[20] M. Berger, P. Colella. *J. comput. Phys.*, **64**, 64 (1989).
[21] G. Carey, M. Anderson, B. Cames, B. Kirk. *J. comput. appl. Math.*, **166**, 55 (2004).
[22] P. Colella, M. Dorr, D. Wake. *J. comput. Phys.*, **152**, 550 (1999).
[23] L. Ferm, P. Lötstedt. *AIAA J.*, **37**, 121 (1999).
[24] A. Madzvamuse, R. Thomas, P.K. Maini, A.J. Wathen. *Bull. math. Biol.*, **64**, 501 (2002).
[25] M. Walkley, P.K. Jimack, M. Berzins. *Int. J. numer. Meth. Fl.*, **40**, 551 (2002).
[26] I.W. Stewart. *The Static and Dynamic Continuum Theory of Liquid Crystals*. Taylor & Francis, London (2004).
[27] P. de Gennes. *Mol. Cryst. liq. Cryst.*, **129**, 193 (1971).
[28] C. de Boor. In *Conference on the Applications of Numerical Analysis* Dundee 1973, J. Morris (Ed.). Vol. 363 of Lecture Notes in Mathematics, Springer-Verlag, Berlin (1974).
[29] M.G. Beckett, J.A. Mackenzie, A. Ramage, D.M. Sloan. *J. comput. Phys.*, **167**, 372 (2001).
[30] L.S. Mulholland, Y. Qiu, D.M. Sloan. *J. comput. Phys.*, **131**, 280 (1997).
[31] W. Ren, X.-P. Wang. *J. comput. Phys.*, **159**, 246 (2000).
[32] J.M. Sanz-Serna, I. Christie. *J. comput. Phys.*, **67**, 348 (1986).
[33] COMSOL Group, *COMSOL multiphysics™,* http://www.comsol.com/, version 3.2 (2006).
[34] A. Ramage, C.J. Newton. *Moving mesh methods for liquid crystal device modelling: A one-dimensional feasibility study,* Tech. Rep. 13/06, University of Strathclyde (2006).
[35] G. Boyd, J. Cheng, P. Ngo. *Appl. Phys. Lett.*, **36**, 556 (1980).

Downloaded At: 15:44 25 January 2011